Hydrol. Earth Syst. Sci., 13, 2399–2412, 2009
www.hydrol-earth-syst-sci.net/13/2399/2009/

Hydrology and Earth System Sciences

Reducing scale dependence in TOPMODEL using a dimensionless topographic index

A. Ducharne

Laboratoire Sisyphe, CNRS/UPMC, Paris, France

Received: 28 January 2009 – Published in Hydrol. Earth Syst. Sci. Discuss.: 4 March 2009
Revised: 6 November 2009 – Accepted: 10 November 2009 – Published: 14 December 2009

Abstract. This paper stems from the fact that the topographic index used in TOPMODEL is not dimensionless. In each pixel i in a catchment, it is defined as $x_i = \ln(a_i/S_i)$, where a_i is the specific contributing area per unit contour length and S_i is the topographic slope. In the SI unit system, a_i/S_i is in meters, and the unit of x_i is problematic. We propose a simple solution in the widespread cases where the topographic index is computed from a regular raster digital elevation model (DEM). The pixel length C being constant, we can define a dimensionless topographic index $y_i = x_i - \ln C$. Reformulating TOPMODEL equations to use y_i instead of x_i helps giving the units of all their terms and emphasizes the scale dependence of these equations via the explicit use of C outside from the topographic index, in what can be defined as the transmissivity at saturation per unit contour length T_0/C. The term $\ln C$ defines the numerical effect of DEM resolution, which contributes to shift the spatial mean $\overline{x}$ of the classical topographic index when the DEM cell size C varies. A key result is that both the spatial mean $\overline{y}$ of the dimensionless index and T_0/C are much more stable with respect to DEM resolution than their counterparts $\overline{x}$ and T_0 in the classical framework. This shows the importance of the numerical effect in the dependence of the classical topographic index to DEM resolution, and reduces the need to recalibrate TOPMODEL when changing DEM resolution.

1 Introduction

TOPMODEL was originally introduced by Beven and Kirkby (1979) as a conceptual rainfall-runoff model, describing the contributions of both saturation excess flow and baseflow from the saturated zone to the catchment outflow. Simplifying assumptions, widely known as TOPMODEL's assumptions, allow one to relate the spatial distribution of the water table depth to the one of a topographic index (TI), depending in each point of the catchment upon local slope, upslope contributing area, and downslope contour length. This distribution of the water table depth controls (i) baseflow owing to the physically-based Darcy's law, and (ii) the extent of the surface saturated area, thus the saturation excess flow, owing to the variable contributing area concept first proposed by Cappus (1960).

This model has been widely used, and not only as a rainfall-runoff model. As high values of the TI reflect a high potential for local saturation, maps of this index have been used to delineate wetlands (e.g. Mérot et al., 1995; Curie et al., 2007). Over the last decade, TOPMODEL's concepts have also been increasingly used in land surface models to describe the influence of topography on the lateral heterogeneity of runoff, soil moisture, and the coupled surface energy balance, including evapotranspiration (e.g. Famiglietti and Wood, 1994; Peters-Lidard et al., 1997; Stieglitz et al., 1997; Koster et al., 2000; Ducharne et al., 2000; Chen and Kumar, 2001; Decharme and Douville, 2006).

The high popularity of TOPMODEL arises from its simplicity of use, especially since topography has become widely described by digital elevation models (DEMs) from which it is easy to compute the TI. A recurring issue, however, is that the TI distribution is markedly impacted by the topographic information content of DEMs, which depends both on the scale of the topographic map the DEM is derived from (Wolock and Price, 1994), and on the DEM resolution, as defined by the pixel size.

The first-order effect of DEM resolution is known as the translation or shift effect, which consists in an increase of mean TI when the DEM resolution decreases, i.e. with coarser cell sizes. This shift effect has been underlined by many studies, from Quinn et al. (1991); Zhang and Montgomery (1994); Bruneau et al. (1995) to Valeo and Moin

Correspondence to: A. Ducharne
(agnes.ducharne@upmc.fr)

(2000); Wu et al. (2007). This increase in mean TI has important hydrological consequences since it imposes to simultaneously decrease the effective value of transmissivity to preserve the hydrological performance of TOPMODEL, as first showed by Franchini et al. (1996) and detailed in Sect. 4.1. In this framework, many efforts have dealt with detailed geomorphological analyses to understand the complex relationships between DEM resolution and the TI or its components, namely the local slope and the specific upslope contributing area (e.g. Wolock and Price, 1994; Sørensen and Seibert, 2007), and to formalize these empirical relationships into scaling functions (e.g. Saulnier et al., 1997b; Wolock and McCabe, 2000; Ibbitt and Woods, 2004; Pradhan et al., 2006).

This paper addresses the scaling issues related to the TI from a different perspective. A reminder of the TOPMODEL framework in Sect. 2 leads us to the starting point of this analysis: the TI is not dimensionless but it is the logarithm of a ratio dimensioned in meters. In Sect. 3, we show how this ratio explicitly depends on DEM resolution when topography is described by a raster DEM, as in most present time applications of TOPMODEL. We further show how we can define a dimensionless TI, which is free from this mathematical dependence, and how we can easily rearrange the equations of TOPMODEL to use this dimensionless TI. This does not change TOPMODEL at all, but this new formalism helps to better understand the scale issues in TOPMODEL, as shown in Sect. 4, from a theoretical point of view, then based on real-world case studies, then by comparison with published rescaling techniques.

2 Classical TOPMODEL's development

The following development of TOPMODEL equations from its simplifying assumptions is not new and was inspired by many papers, in particular from Beven and Kirkby (1979), Sivapalan et al. (1987), Franchini et al. (1996) and Stieglitz et al. (1997). All notations are defined in Table 1 with their SI unit.

2.1 Scope and assumptions

Let us consider a hydrological catchment of area A. Let us further assume that the topography of this catchment is described by a raster DEM with a pixel length C so that $A{=}nC^2$, n being the number of pixels in the catchment.

To describe the evolution of the water table depth over time and space, which is crucial to predict baseflow from this water table and the extent of saturated areas thus saturation excess flow, TOPMODEL relies on four strong assumptions H1 to H4 regarding the behaviour of the modelled catchment:

H1: at each time step, the recharge to the water table, $R(t)$, is uniform in the catchment.

H2: the water table dynamics is approximated by a succession of steady states, so that in each pixel of the catchment and at each time step, the local outflow from the saturated zone equals the recharge from the contributing area. Isolating one time step, over which the uniform recharge rate is R, we can thus write Q_i, the outflow from the saturated zone at any pixel i in the catchment, as

$$Q_i = A_i R \tag{1}$$

where A_i is the local contributing area.

H3: in each pixel i, the local hydraulic gradient is approximated by the local topographic slope S_i.

H4: the saturated hydraulic conductivity K_s is uniform in the catchment but decreases with depth following an exponential law:

$$K_s(z) = K_0 \exp(-\nu z) \tag{2}$$

where z is the depth from the soil surface, $K_0 = K_s(z = 0)$ is the saturated hydraulic conductivity at the soil surface, and ν is the saturated hydraulic conductivity decay factor with depth. Both K_0 and ν are uniform in the catchment.

Assumption H4 has been relaxed by Ambroise et al. (1996) and Duan and Miller (1997) regarding the shape of the vertical profile of saturated hydraulic conductivity, and by Beven (1986) regarding the uniformity of K_0. Assumption H2 has been relaxed by Beven and Freer (2001a) using a kinematic wave routing of subsurface flow. Assumption H3, pertaining to the local hydraulic gradient, can also be relaxed, using the concept of reference levels (Quinn et al., 1991). Assumption H1, however, is essential to derive the simple relationship between the local and mean water depths which is at the crux of TOPMODEL (Eq. 13). The only way to relax it is to separate different landscape or hillslope elements within the catchment, as already proposed in the seminal paper by Beven and Kirkby (1979) and further developed in the finely distributed application of TOPMODEL of Peters-Lidard et al. (1997). For simplicity, we will stick in the following to the original assumptions.

2.2 Towards TOPMODEL equations

From Darcy's law and assumption H3, the local outflow from the saturated zone at pixel i, across a downstream edge of length L_i, can be written

$$Q_i = L_i T_i S_i. \tag{3}$$

In this expression, T_i is the local transmissivity defined as

$$T_i = \int_{z_i}^{\infty} K_s(z) dz \tag{4}$$

Table 1. Notations and units (pertaining to Sects. 2 and 3.1).

Variable	SI unit	Description
a_i	m	Specific contributing area per unit contour length
a_{out}	m	Specific contributing area per unit contour length at the outlet ($a_{out} = A/L_{out}$)
A	m^2	Catchment area
A_i	m^2	Contributing area at pixel i
C	m	DEM resolution (pixel length)
h_i	m	Local altitude at pixel i
K_s	$m\,s^{-1}$	Saturated hydraulic conductivity
K_0	$m\,s^{-1}$	Saturated hydraulic conductivity at the surface
L_i	m	Downhill contour length at pixel i
L_{out}	m	Downhill contour length at the outlet pixel
n	–	Number of pixels in the catchment
n_i	–	Local number of upslope pixels at pixel i
n_{out}	–	Local number of upslope pixels at the outlet ($n = n_{out}$)
p_i	m	Local piezometric head at pixel i
Q_i	$m^3\,s^{-1}$	Outflow from the saturated zone at pixel i
Q_{out}	$m^3\,s^{-1}$	Outflow from the saturated zone at the outlet, or baseflow from the catchment
R	$m\,s^{-1}$	Uniform recharge rate in the catchment
S_i	–	Local topographic slope at pixel i
S_{out}	–	Local topographic slope at the outlet
T_i	$m^2\,s^{-1}$	Local transmissivity of the saturated zone at pixel i
T_0	$m^2\,s^{-1}$	Local transmissivity at saturation, assumed uniform in the catchment (H4)
x_i	ln(m)	Classical topographic index at pixel i
x_{out}	ln(m)	Classical topographic index at the outlet
$\overline{x}$	ln(m)	Catchment average of the classical topographic index
y_i	–	Dimensionless topographic index at pixel i
y_{out}	–	Dimensionless topographic index at the outlet
$\overline{y}$	–	Catchment average of the dimensionless topographic index
z_i	m	Local water table depth at pixel i
z_{out}	m	Local water table depth at the outlet
$\overline{z}$	m	Catchment average of the water table depth
ν	m^{-1}	Saturated hydraulic conductivity decay factor with depth

where z_i is the local depth to the water table. Combining with Eq. (2), we get

$$T_i = K_0 \int_{z_i}^{\infty} e^{-\nu z} dz = \frac{K_0}{\nu} \exp(-\nu z_i) = T_0 \exp(-\nu z_i) \quad (5)$$

where $T_0 = K_0/\nu$ is the transmissivity of the soil when it is fully saturated (z_i=0). Combining Eqs. (1), (3) and (5) leads to

$$Q_i = A_i R = L_i T_0 S_i \exp(-\nu z_i). \quad (6)$$

Under TOPMODEL's assumptions, this holds everywhere in the catchment, in particular at the outlet which drains the entire catchment. The baseflow from the catchment is thus

$$Q_{out} = L_{out} T_0 S_{out} \exp(-\nu z_{out}) \quad (7)$$

where the only unknown is z_{out}, the water table depth at the outlet pixel where the local slope is S_{out}. More generally, the distribution of the local water table depth z_i in the catchment is used to deduce the surface saturated area, which is defined by the pixels where $z_i \leq 0$. Rewriting Eq. (6), z_i can be expressed as follows:

$$z_i = -\frac{1}{\nu} \ln\left(\frac{A_i R}{L_i T_0 S_i}\right). \quad (8)$$

Introducing $a_i = A_i/L_i$, the specific contributing area per unit contour length, we find the classical TOPMODEL equation, where the fraction in the natural logarithm is dimensionless:

$$z_i = -\frac{1}{\nu} \ln\left(\frac{a_i R}{T_0 S_i}\right). \quad (9)$$

Separating, in the natural logarithm, the variables that are uniform in the catchment from the ones that are not, we get

$$z_i = -\frac{1}{\nu} \left(\ln\frac{R}{T_0} + \ln\frac{a_i}{S_i}\right). \quad (10)$$

The variable term is defined in TOPMODEL as the topographic index (TI):

$$x_i = \ln \frac{a_i}{S_i}. \quad (11)$$

Note that relaxing the assumption that K_0 is uniform leads to another index of lateral heterogeneity (Beven, 1986), the soil-topographic index $\ln(a_i/T_i S_i)$. In any case, the ratio on which the natural logarithm is applied is not dimensionless. The mean water table depth $\overline{z}$ is introduced to eliminate the uniform term:

$$\overline{z} = -\frac{1}{\nu}\left(\ln(\frac{R}{T_0}) + \overline{x}\right) \quad (12)$$

so that

$$z_i - \overline{z} = -\frac{1}{\nu}(x_i - \overline{x}) \quad (13)$$

where $\overline{x}$ is the average of x_i over the catchment. This equation, which states that the spatial variations of the water table and the TI are proportional, is probably the most important in the TOPMODEL framework. It is used to deduce the surface saturated area from the distribution of x_i in the catchment and the mean table depth $\overline{z}$. Applied to the outlet pixel, with local water table depth and TI z_{out} and x_{out}, it also gives

$$z_{\text{out}} = \overline{z} - \frac{1}{\nu}(x_{\text{out}} - \overline{x}) \quad (14)$$

which, substituted in Eq. (7), leads to

$$\begin{aligned} Q_{\text{out}} &= L_{\text{out}} T_0 S_{\text{out}} \exp(-\nu\overline{z} + x_{\text{out}} - \overline{x}) \\ &= L_{\text{out}} T_0 S_{\text{out}} \exp(\ln \frac{a_{\text{out}}}{S_{\text{out}}}) \exp(-\nu\overline{z} - \overline{x}) \\ &= a_{\text{out}} L_{\text{out}} T_0 \exp(-\nu\overline{z} - \overline{x}) \end{aligned}$$

$$Q_{\text{out}} = A T_0 \exp(-\nu\overline{z} - \overline{x}). \quad (15)$$

Using SI units, AT_0 is in $\text{m}^4\,\text{s}^{-1}$, but Q_{out} is in $\text{m}^3\,\text{s}^{-1}$. This results from the fact that $\exp(-\overline{x})$ is in m^{-1}, since x_i is the natural logarithm of a ratio dimensioned in m. Even if Eqs. (10), (12), (13) and (15) are homogeneous, using the logarithm of a non-dimensionless quantity as an index might be confusing. We thus introduce a dimensionless TI, which solves this dimension issue and helps to understand the scale issues related to DEM resolution, as developed in the following.

3 Introducing a dimensionless TI

3.1 Topographic analysis using single-flow direction algorithms

Many methods are available for deriving the slopes S_i, upslope contributing areas A_i, and downhill contour length L_i, from a regular raster DEM. The most simple ones are the single-flow direction (SFD) algorithms, according to which one pixel contributes to only one downslope pixel (e.g. Wolock and Price, 1994). These algorithms rely on the digital terrain analysis (DTA) methods introduced by Jenson and Domingue (1988) and are still very popular (e.g. Wolock and McCabe, 2000; Kumar et al., 2000). In this framework, having defined C as the DEM cell size thus pixel length, we can write that $L_i = C$ and $A_i = n_i C^2$, where n_i is the number of pixels in the contributing area. This leads to

$$x_i = \ln \frac{n_i C}{S_i}. \quad (16)$$

The pixel length C being a constant, we can thus introduce a dimensionless topographic index

$$y_i = \ln \frac{n_i}{S_i} \quad (17)$$

which simply relates to x_i

$$x_i = y_i + \ln C. \quad (18)$$

Dimensionless does not mean scale independent and both y_i and x_i depend on DEM resolution, which controls n_i and S_i (e.g. Wolock and McCabe, 2000; Sørensen and Seibert, 2007). Equation (18), however, shows that the classical TI x_i is subjected to an additional influence from DEM resolution, explicited by the term $\ln C$. This term is responsible of the numerical effect detailed in Sect. 4.1, which contributes to shift the mean classical TI $\overline{x}$ when DEM resolution varies.

Section 3.2 will show how Eqs. (17) and (18) can be generalized to the more complex cases where multiple-flow direction algorithms (e.g. Quinn et al., 1991) are used to compute a_i, L_i and S_i. In any case, Eq. (10) becomes

$$z_i = -\frac{1}{\nu}\left(\ln(\frac{CR}{T_0}) + y_i\right) \quad (19)$$

where the natural logarithm is applied to two dimensionless terms. In addition, the DEM resolution is explicited via C.

From there, we can follow the same development with this index as in TOPMODEL with x_i and introduce the mean water table depth $\overline{z}$ to eliminate the uniform term:

$$z_i - \overline{z} = -\frac{1}{\nu}(y_i - \overline{y}) \quad (20)$$

where $\overline{y}$ is the average of y_i over the catchment. Applied to the outlet pixel, it gives

$$z_{\text{out}} = \overline{z} - \frac{1}{\nu}(y_{\text{out}} - \overline{y}) \quad (21)$$

which, substituted in Eq. (7), leads to

$$\begin{aligned} Q_{\text{out}} &= C T_0 S_{\text{out}} \exp(-\nu\overline{z} + y_{\text{out}} - \overline{y}) \\ &= C T_0 S_{\text{out}} \exp(\ln \frac{n_{\text{out}}}{S_{\text{out}}}) \exp(-\nu\overline{z} - \overline{y}) \\ &= n_{\text{out}} C T_0 \exp(-\nu\overline{z} - \overline{y}) \end{aligned}$$

$$Q_{\text{out}} = \frac{A T_0}{C} \exp(-\nu \overline{z} - \overline{y}). \quad (22)$$

This expression is of course perfectly equivalent to Eq. (15), except that it relies on a dimensionless TI y, and that the scale dependence of this expression explicitly appears via the DEM cell size C.

3.2 Generalization to multiple-flow direction algorithms

Since their introduction by Quinn et al. (1991), multiple-flow direction (MFD) algorithms have been widely used to compute the TI and regularly improved (e.g. Holmgren, 1994; Quinn et al., 1995; Seibert and McGlynn, 2006). Their basic difference with SFD algorithms is that they distribute the contribution from the upslope contributing area between all the contiguous downslope cells, proportionally to the corresponding slopes.

In this framework, the expression of the specific area drained per unit contour length is not as simple as the one used with SFD methods, what leads to the following general expression of the TI:

$$x_i = \ln\left(\frac{A_i}{\sum_{d=1}^{n_d} S_i^d L_i^d}\right), \quad (23)$$

where n_d is the total number of downhill directions, S_i^d is the slope between the local pixel i and the neighbouring pixel in the dth downhill direction, and L_i^d is the contour length normal to this direction. Note that this expression also holds for $n_d = 1$, which corresponds to the SFD case.

There are many other variations around the general basis provided by the SFD and MFD methods (e.g. Mendicino and Sole, 1997; Tarboton, 1997). Alternatives also exist regarding the way to account for channel or creek pixels (e.g. Saulnier et al., 1997a; Mendicino and Sole, 1997; Sørensen et al., 2006) or the way to determine flow direction and slope in flat areas (e.g. Wolock and McCabe, 1995; Pan et al., 2004; Gascoin et al., 2009). Several papers addressed the comparison of the various DTA methods to derive the TI (Wolock and McCabe, 1995; Mendicino and Sole, 1997; Pan et al., 2004; Sørensen et al., 2006). They all demonstrate the sensitivity of the TI distribution (including the mean TI $\overline{x}$) to these methods, but their conclusions regarding the relative performances of the different methods are not consistent, apart from a consensus about the superiority of MFD algorithms for divergent hillslopes.

In any case, one can always write that $A_i = \alpha_i C^2$ and $L_i^d = \beta_i^d C$, where α_i and β_i^d are dimensionless factors. This leads to the general form of the TI

$$x_i = \ln\left(\frac{\alpha_i C}{\sum_{d=1}^{n_d} S_i^d \beta_i^d}\right) \quad (24)$$

which can be reduced to the dimensionless TI

$$y_i = \ln\left(\frac{\alpha_i}{\sum_{d=1}^{n_d} S_i^d \beta_i^d}\right) = x_i - \ln C \quad (25)$$

owing to the fact that the pixel length C is constant in regular raster DEMs.

3.3 Generalization to alternative transmissivity profiles

Ambroise et al. (1996) generalized TOPMODEL to use linear and parabolic transmissivity profiles, which, according to the analysis of recession curves by Tallaksen (1995), may be better suited in some cases than the classical exponential profile (Eq. 5). Duan and Miller (1997) built upon this work to propose a fully generalized power function for the transmissivity profile, that can be formulated as follows:

$$T_i = T_0 \left(1 - \frac{\nu}{b} z_i\right)^b. \quad (26)$$

The only new variable is b, which is is a non-dimensional parameter, uniform throughout the catchment, introduced to generalize the solution of Ambroise et al. (1996). In this framework, the decrease of T_0 with depth is controlled by the ratio ν/b rather than by ν. This generalized power function contains the full range of potential transmissivities, from linear when b=1 to exponential when $b \to \infty$. The classical topographic index becomes

$$x_i = \left(\frac{a_i}{S_i}\right)^{1/b}, \quad (27)$$

the local water table depth z_i follows

$$\frac{1 - \frac{\nu}{b} z_i}{1 - \frac{\nu}{b} \overline{z}} = \frac{x_i}{\overline{x}}, \quad (28)$$

and the baseflow at the outlet of the catchment is

$$Q_{\text{out}} = A T_0 \left(\frac{1 - \frac{\nu}{b} \overline{z}}{\overline{y}}\right)^b. \quad (29)$$

A dimensionless index can also be defined in this generalized framework:

$$y_i = \frac{x_i}{C^{1/b}}, \quad (30)$$

and the expressions of the local water table depth and baseflow become

$$\frac{1 - \frac{\nu}{b} z_i}{1 - \frac{\nu}{b} \overline{z}} = \frac{y_i}{\overline{y}} \quad (31)$$

and

$$Q_{\text{out}} = \frac{A T_0}{C} \left(\frac{1 - \frac{\nu}{b} \overline{z}}{\overline{x}}\right)^b, \quad (32)$$

which again shows up the saturated transmissivity per unit contour length T_0/C.

4 Implications regarding scale issues in TOPMODEL

4.1 Attribution of scale effects on the TI distribution and TOPMODEL parameters

Following Zhang and Montgomery (1994), Franchini et al. (1996) showed that the increase in $\overline{x}$ when DEM resolution gets coarser had hydrological consequences, as it had to be offset by larger calibrated transmissivities in TOPMODEL. In a given catchment, two DEMs with different cell sizes $C_2 > C_1$ correspond to different mean TIs $\overline{x_2} > \overline{x_1}$, what is known as the shift effect. If the calibrated value of TOPMODEL's transmissivity is $T_{0,1}$ for cell size C_1, the shift effect can be compensated by a simple recalibration of this transmissivity to $T_{0,2}$, such as to maintain the relationship between the mean water table depth $\overline{z^*}$ and TOPMODEL's baseflow Q^*:

$$Q^* = A\,T_{0,1}\exp(-\nu\overline{z^*} - \overline{x_1}) = A\,T_{0,2}\exp(-\nu\overline{z^*} - \overline{x_2}). \quad (33)$$

Following Franchini et al. (1996), we assume constant ν for simplicity. This leads to the following relationship, which explains the interplay between the calibrated transmissivities and mean TIs:

$$T_{0,2} = T_{0,1}\exp(\overline{x_2} - \overline{x_1}). \quad (34)$$

The dimensionless index y is very much inspired by this pioneering work of Franchini et al. (1996). It also offers a deeper insight on this important interplay between mean TI and calibrated transmissivity. Applying Eq. (18) reveals the direct influence of the change in C onto the change in mean classical TIs:

$$(\overline{x_2} - \overline{x_1}) = \ln\frac{C_2}{C_1} + (\overline{y_2} - \overline{y_1}). \quad (35)$$

It also allows one to explicitly describe this direct DEM influence in Eq. (34), otherwise unchanged:

$$T_{0,2} = T_{0,1}\frac{C_2}{C_1}\exp(\overline{y_2} - \overline{y_1}), \quad (36)$$

what leads to generalize this relationship to the transmissivity per unit contour length:

$$\frac{T_{0,2}}{C_2} = \frac{T_{0,1}}{C_1}\exp(\overline{y_2} - \overline{y_1}). \quad (37)$$

Of course, $(\overline{y_2} - \overline{y_1})$ also depend on DEM resolution. Equations (35) and (36) thus show that the changes in mean classical TI $\overline{x}$ and calibrated T_0 when the DEM resolution varies arise from two different causes, as also summarized in Table 2:

- a numerical effect, because the DEM cell size mathematically C enters into the expression of a_i. Using the dimensionless TI allows one to identify this numerical effect (Eq. 35), which changes $\overline{x}$ by $\ln(C_2/C_1)$ and T_0 by the scaling factor C_2/C_1;
- a terrain effect, owing to the influence of DEM resolution on both the local slopes S_i and the shape of the hydrographic network, thus n_i and a_i. Following Wolock and McCabe (2000), this terrain effect can itself be separated in two components: a discretization effect, which arises from dividing the terrain in different numbers of grid cells; and a smoothing effect, related to decreased variability of the local slopes when using coarser resolution DEMs, what filters the terrain roughness (Valeo and Moin, 2000).

  These terrain effects, which concern both the classical and dimensionless TI, have consequences on the shape of the TI distribution and on its mean. The effect on the mean contributes to the shift effect, and its consequence on the calibrated T_0 is isolated in the term $\exp(\overline{y_2} - \overline{y_1})$ of Eq. (36). Note that this effect also influences the transmissivity per unit contour length T_0/C, owing to the interplay between the latter and the mean dimensionless TI (Eq. 37).

To summarize this theoretical analysis, the influence of DEM resolution on the shape of the TI distribution is shared by the classical and dimensionless TIs. In contrast, $\overline{y}$ and the transmissivity per unit contour length T_0/C are probably less sensitive to DEM resolution than their counterparts in the classical formulation, $\overline{x}$ and T_0, because the former only depend on the terrain effects, whereas the latter also depend on the numerical effect. This is further investigated based on real-world case studies.

4.2 Importance of the numerical effect in real-world case studies

In the extensive literature devoted to the influence of DEM resolution onto the classical TI distribution and the performances of TOPMODEL, we could find six papers allowing us to calculate the mean of the dimensionless index $\overline{y}$ for different DEM cell sizes C. The six corresponding case studies are briefly summarized in Table 3. Note that the Maurets catchment (Saulnier et al., 1997b) is a subcatchment of the experimental research catchment of the Réal Collobrier (Franchini et al., 1996), and that mean TIs from two different DTAs, namely the SFD and MFD algorithms, are available in the sub-catchment W3 of the Sleepers River (Wolock and McCabe, 1995).

In the six case studies, TOPMODEL was calibrated for each of the different tested DEM resolutions, to optimize the fit between predicted and observed discharge. The goodness-of-fit criterion was the Nash and Sutcliffe (1970) efficiency, except in the Réal Collobrier where it was the correlation coefficient between the simulated and observed discharge. The calibration always addressed the surface saturated hydraulic conductivity K_0, but was not systematic for the other parameters, namely ν, the decay factor of K_0 with depth, and SRmax, the water capacity of the interception and root zone

Table 2. DEM resolution effects in the classical TOPMODEL framework: separation of the different effects on the TI distribution, and quantification of the related changes in mean TI $\overline{x}$ vs. transmissivity T_0. Following Eqs. (36) and (35), the grid cell size is assumed to vary from C_1 to C_2, with subsequent changes in the mean dimensionless TI from $\overline{y_1}$ to $\overline{y_2}$.

DEM resolution effects		Influence on TI distribution: Shape	Influence on TI distribution: $\overline{x}$ (Shift effect)	Quantified effect on $\overline{x}$	Quantified effect on T_0
Numerical			×	$\ln(C_2/C_1)$	C_2/C_1
Terrain	Discretization	×	×	$\overline{y_2}-\overline{y_1}$	$\exp(\overline{y_2}-\overline{y_1})$
	Smoothing	×	×		

Table 3. Main features of the selected case studies. DTA means Digital Terrain Analysis, and SFD and MFD stand for single and multiple-flow direction algorithms. NA=Not Available.

Catchment	Reference	Location	Area (km^2)	Altitude range (m)	Map scale	Min(C)	Max(C)	DTA method
Sleepers-W3	Wolock and McCabe (1995)	Vermont, USA	8.4	621	1:24 000	30-m	90-m	SFD and MFD
Réal Collobrier	Franchini et al. (1996)	France	71	700 [a]	NA	60-m	480-m	MFD
Maurets	Saulnier et al. (1997b)	France	8.4	561	1:25 000	20-m	120-m	MFD
Bore Khola	Brasington and Richards (1998)	Nepal	4.5	1290 [b]	1:5000	20-m	500-m	MFD
Haute-Mentue	Higy and Musy (2000)	Switzerland	12	236 [c]	1:25 000	25-m	150-m	MFD [c]
Kamishiiba	Pradhan et al. (2006)	Japan	210	1400 [d]	NA	50-m	1000-m	SFD

[a] from Obled et al. (1994)
[b] from Brasington and Richards (2000)
[c] from Iorgulescu and Jordan (1994)
[d] from Lee et al. (2006)

storage, which controls the recharge term in TOPMODEL (Table 4). Important common features of the six calibration exercises are that similar goodness-of-fit were achieved for all DEM resolutions, and that K_0 was always the most effective parameter to compensate the DEM resolution changes, as shown by the small variation ranges, if any, of ν and SRmax in Table 4.

These case studies confirm that, once chosen the DTA method to compute the TI, the mean of the classical index $\overline{x}$ increases with DEM cell size C (Table 5), a rule that we could not find invalidated in the literature. Based on the values gathered in Table 5, the mean classical TI $\overline{x}$ exhibits variation rates between 0.005 and 0.02, the related unit being $\ln(\mathrm{m})\,\mathrm{m}^{-1}$. In contrast, positive variation rates are not systematic for the mean dimensionless TI $\overline{y}$. This analysis also holds for the correlation coefficients of the mean TIs with DEM resolution, which are not systematically positive and high with $\overline{y}$, whereas they are significantly so with $\overline{x}$.

More importantly, these variation rates show that the mean dimensionless TI $\overline{y}$ varies much less with DEM resolution than does the mean classical TI $\overline{x}$, in all the seven studied cases. This result is further illustrated in Fig. 1, where the trajectories followed by $\overline{y}$ span smaller ranges than the ones followed by $\overline{x}$ under the same DEM resolution changes. Of course, the units are different and there is no point comparing $\overline{x}$ and $\overline{y}$ for the same DEM resolution. Their changes when DEM resolution varies, however, are important as they motivate the rescaling of transmissivity (Sect. 4.1).

Figure 1 also shows that the variations of $\overline{x}$ due to DEM resolution are primarily logarithmic, and exceed the ones related to the DTA methods and the location of the catchments, which controls their specific topographical features. As a result, one cannot isolate the different locations from the variability induced on $\overline{x}$ by the DEM resolution. In contrast, one can separate the projections of the different trajectories on the vertical axis representing $\overline{y}$, what shows that the mean dimensionless TI can efficiently discriminate the different locations, regardless of DEM resolution.

This is illustrated by the correlations between the altitude range and the mean TIs of the six selected catchments (Fig. 2). Fixing the DEM resolution, this correlation is highly negative with the mean of both TIs, what probably results from the fact that local slopes are higher in catchments with an important altitude range. The comparison of the two

Table 4. Summary of the calibration method and results in the six selected case studies (see Table 3). The goodness-of-fit criterion is the Nash and Sutcliffe (1970) efficiency, except in the Réal Collobrier where it is the correlation coefficient between the simulated and observed discharge. In each case, bold figures indicate the parameters that were calibrated to compensate for the DEM resolution changes. NCP=Number of calibrated parameters, NA=Not Available.

Catchment	Calibration method				Calibration results			
	Period	Time step (h)	DEM resolution range (m)	NCP	K_0 range (m/h)	ν range (m^{-1})	SRmax range (mm)	Efficiency range
Sleepers-W3	1 year	24	30–90	2	**0.018–0.034**	**3.3–3.6**	NA	0.88–0.89
Réal Collobrier	3 months	1	60–480	1	**35–700**	58.8	22	0.96*
Maurets	11 storms of 10 to 24 days	0.5	20–120	3	**82–1402**	**38.5–40**	**19–21**	0.83
Bore Khola	1 month	0.5	20–500	3	**18–198**	**14–19.2**	**3.6–5.8**	0.72–0.74
Haute-Mentue	28 days with 2 storms	1	25–150	2	**27–118**	**22.8–29.2**	20	0.79–0.82
Kamishiiba	1 storm of 120 h	NA	50–1000	1	**86–2858**	1.43	1	0.96

* Correlation coefficient

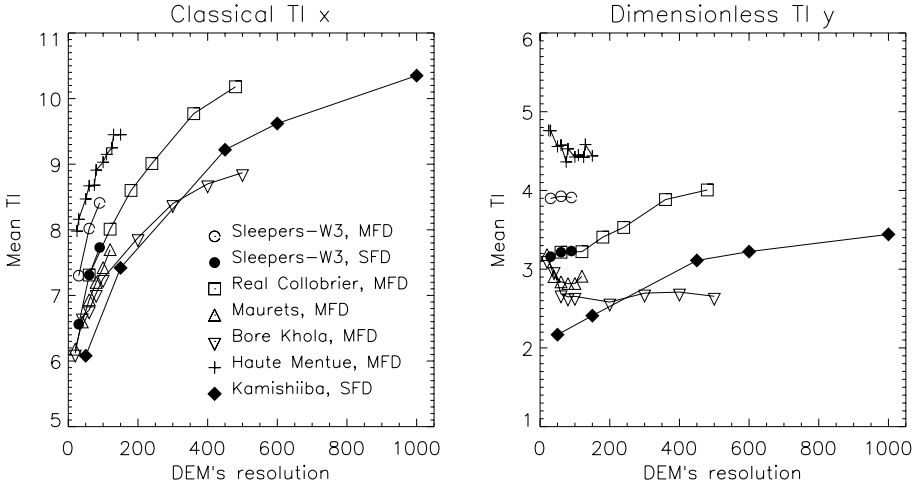

Fig. 1. Relationships between mean TI and DEM resolution, in the classical and dimensionless TOPMODEL frameworks. Values come from Table 5, which also gives the corresponding correlation coefficients.

panels in Fig. 2, however, shows that if care is not taken to use the same DEM resolution when comparing mean TIs between catchments, the relationship between mean TI and altitude range is completely hidden with $\overline{x}$ whereas it is detectable with $\overline{y}$.

The above results are linked to the fact that, at least in the selected catchments, the shift effect on $\overline{x}$ is largely dominated by the logarithmic numerical effect, which is absent by construction when using the dimensionless TI. The DEM effects that remain in the variations of $\overline{y}$ are the terrain effects (Sect. 4.1), so that it is advisable to study them on this dimensionless TI rather than on the classical one, where they are largely hidden by the numerical effect. This is illustrated in the right panel of Fig. 1, which shows that these terrain effects have contrasted signatures in the different catchments, with a positive dependence on DEM resolution in only half of them (Sleepers-W3, Réal Collobrier, Kamishiiba).

The case studies also reveal that T_0/C varies much less with DEM resolution than its counterpart T_0 in the classical framework (Fig. 3 and Table 6). This is a direct consequence of the interplay between mean TI and transmissivity (Eq. 36), given that the terrain effects, quantified by $\exp(\overline{y_2}-\overline{y_1})$, are small enough compared to the numerical effect C_2/C_1 to be neglected at first order. As a result, Eq. (37) can be approximated by

$$\frac{T_{0,2}}{C_2} \simeq \frac{T_{0,1}}{C_1}. \tag{38}$$

Table 5. Mean TIs $\overline{x}$ (in ln(m)) and $\overline{y}$ (dimensionless) for six different catchments and different DEM resolutions (cell sizes in m). The reported values come from the literature (see Table 3). The last two columns give: the mean variation rates of $\overline{x}$ and $\overline{y}$ with DEM resolution, in ln(m) m^{-1} and m^{-1}, respectively; the Spearman's rank correlation coefficients ρ between the mean TIs and DEM resolution, the star indicating a significant correlation at the risk α=0.05.

Sleepers-W3 (Wolock and McCabe, 1995)													
Resolution	30	60	90									$\Delta/\Delta C$	ρ
$\overline{x}$	6.56	7.31	7.73	(SFD)								0.020	1.00*
$\overline{y}$	**3.16**	**3.22**	**3.23**	(SFD)								**0.001**	**1.00***
$\overline{x}$	7.30	8.02	8.41	(MFD)								0.019	1.00*
$\overline{y}$	**3.90**	**3.93**	**3.91**	(MFD)								**0.000**	**0.50**
Réal Collobrier (Franchini et al., 1996)													
Resolution	60	120	180	240	360	480						$\Delta/\Delta C$	ρ
$\overline{x}$	7.31	8.01	8.60	9.01	9.77	10.18						0.006	1.00*
$\overline{y}$	**3.22**	**3.22**	**3.41**	**3.53**	**3.88**	**4.00**						**0.002**	**1.00***
Maurets (Saulnier et al., 1997b)													
Resolution	20	40	60	80	100	120						$\Delta/\Delta C$	ρ
$\overline{x}$	6.18	6.60	6.93	7.20	7.42	7.70						0.015	1.00*
$\overline{y}$	**3.18**	**2.90**	**2.84**	**2.82**	**2.82**	**2.91**						**−0.002**	**−0.37**
Bore Khola (Brasington and Richards, 1998)													
Resolution	20	40	60	80	100	200	300	400	500			$\Delta/\Delta C$	ρ
$\overline{x}$	6.12	6.67	6.78	7.03	7.26	7.88	8.40	8.70	8.87			0.006	1.00*
$\overline{y}$	**3.12**	**2.98**	**2.69**	**2.65**	**2.65**	**2.58**	**2.70**	**2.71**	**2.66**			**−0.001**	**−0.36**
Haute-Mentue (Higy and Musy, 2000)													
Resolution	25	30	50	60	75	80	100	110	125	130	150	$\Delta/\Delta C$	ρ
$\overline{x}$	7.98	8.16	8.47	8.67	8.68	8.91	9.03	9.15	9.25	9.45	9.45	0.011	0.99*
$\overline{y}$	**4.76**	**4.76**	**4.56**	**4.58**	**4.36**	**4.53**	**4.42**	**4.45**	**4.42**	**4.58**	**4.44**	**−0.000**	**−0.52**
Kamishiiba (Pradhan et al., 2006)													
Resolution	50	150	450	600	1000							$\Delta/\Delta C$	ρ
$\overline{x}$	6.08	7.42	9.22	9.62	10.35							0.005	1.00*
$\overline{y}$	**2.17**	**2.41**	**3.11**	**3.22**	**3.44**							**0.000**	**1.00***

Note that this does not imply that T_0/C is independent from DEM resolution. Among the four catchments where it makes sense to quantify the correlation between T_0/C and DEM resolution (catchments with more than three calibrated T_0), two of them exhibit a positive and significant correlation. In one of them, the Maurets catchment, this cannot be simply attributed to the terrain effects, as there is no significant correlation between the mean dimensionless index $\overline{y}$ and DEM resolution (Table 5). The dependence of T_0 on DEM resolution is actually more complicated than the one of $\overline{x}$ or $\overline{y}$, as it is a calibrated parameter, with an important related uncertainty. As shown using the GLUE (Generalized Likelihood uncertainty Estimation) methodology for instance, calibration does not allow one to identify a unique optimal set of parameters, and in the special case of T_0, equally good results can be achieved with values ranging over orders of magnitude (e.g. Beven and Binley, 1992; Freer et al., 1996; Beven and Freer, 2001b; Gallart et al., 2007). Yet, using the dimensionless framework reduces the need to recalibrate TOPMODEL when DEM resolution varies, as T_0/C becomes an explicit parameter, namely the transmissivity at saturation per unit contour length (Eq. 22), which depends much less on DEM resolution than T_0 despite the above uncertainties.

4.3 Comparison with alternative rescaling techniques

4.3.1 Rescaling of transmissivity

Given the interplay between mean classical TI and transmissivity, Franchini et al. (1996) concluded that satisfactory performances of TOPMODEL could be achieved when changing DEM resolution by rescaling the transmissivity using Eq. (34). The above results show that a significant part of this rescaling can be achieved without even analyzing the DEM at the new resolution, by simply accounting for the numerical effect (Eq. 38).

Table 6. Calibrated transmissivity T_0 (in $m^2\,h^{-1}$) and its ratio to pixel length T_0/C (in $m\,h^{-1}$) for six different catchments and different DEM resolutions (cell sizes in m). The reported values come from the literature (see Table 3). The last two columns give: the mean variation rates of the parameters with DEM resolution, in $m\,h^{-1}$ for T_0 and in h^{-1} for T_0/C; the Spearman's rank correlation coefficients ρ between the parameters and DEM resolution, the star indicating a significant correlation at the risk α=0.05.

Sleepers-W3 (Wolock and McCabe, 1995)													
Resolution	30	60	90									$\Delta/\Delta C$	ρ
T_0	0.001	0.002	0.003	(SFD)								3. 10^{-5}	1.00*
T_0/C	**3.2 10^{-5}**	**3.7 10^{-5}**	**3.8 10^{-5}**	(SFD)								**1. 10^{-7}**	**1.00***
T_0	0.002	0.004	0.005	(MFD)								5. 10^{-5}	1.00*
T_0/C	**7.0 10^{-5}**	**6.3 10^{-5}**	**5.7 10^{-5}**	**(MFD)**								**$-2.\ 10^{-7}$**	**-1.00***
Réal Collobrier (Franchini et al., 1996)													
Resolution	60	120	180	240	360	480						$\Delta/\Delta C$	ρ
T_0	0.60	1.19	2.55	3.40	7.65	11.90						0.027	1.00*
T_0/C	**0.010**	**0.010**	**0.014**	**0.014**	**0.021**	**0.025**						**0.000**	**0.94***
Maurets (Saulnier et al., 1997b)													
Resolution	20	40	60	80	100	120						$\Delta/\Delta C$	ρ
T_0	2.05	4.60	11.23	21.00	21.37	35.05						0.330	1.00*
T_0/C	**0.10**	**0.12**	**0.19**	**0.26**	**0.21**	**0.29**						**0.002**	**0.94***
Bore Khola (Brasington and Richards, 1998)													
Resolution	20	40	60	80	100	200	300	400	500			$\Delta/\Delta C$	ρ
T_0	0.95	1.36	1.67	1.95	2.46	7.07	7.83	11.86	14.03			0.027	1.00*
T_0/C	**0.048**	**0.034**	**0.028**	**0.024**	**0.025**	**0.035**	**0.026**	**0.030**	**0.028**			**-0.000**	**-0.23**
Haute-Mentue (Higy and Musy, 2000)													
Resolution	25	30	50	60	75	80	100	110	125	130	150	$\Delta/\Delta C$	ρ
T_0	1.13	1.45	1.57	1.91	2.20	3.95	4.19	4.02	4.35	4.87	5.20	0.033	0.99*
T_0/C	**0.05**	**0.05**	**0.03**	**0.03**	**0.03**	**0.05**	**0.04**	**0.04**	**0.03**	**0.04**	**0.03**	**-0.000**	**-0.13**
Kamishiiba (Pradhan et al., 2006)													
Resolution	50	150	450	600	1000							$\Delta/\Delta C$	ρ
T_0	6				200							0.204	1.00*
T_0/C	**0.12**				**0.20**							**0.000**	**1.00***

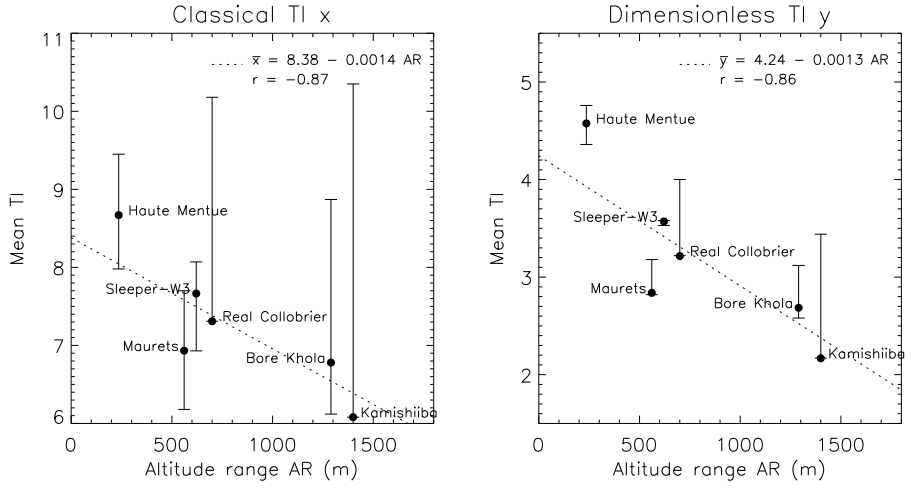

Fig. 2. Relationships between the altitude range (from Table 3) and the mean TIs in the six selected catchments: classical TI on the left panel vs. dimensionless TI on the right panel (values from Table 5). The regression lines and correlation coefficients are computed from the mean TIs at the 60-m resolution, used in all the catchments apart from the Kamishiiba catchment, where the 50-m resolution is used instead. For the Sleepers-W3 catchment, we took the average of the mean TIs from the SFD and MFD algorithms. The vertical bars define the range of mean TIs across the different DEM resolutions.

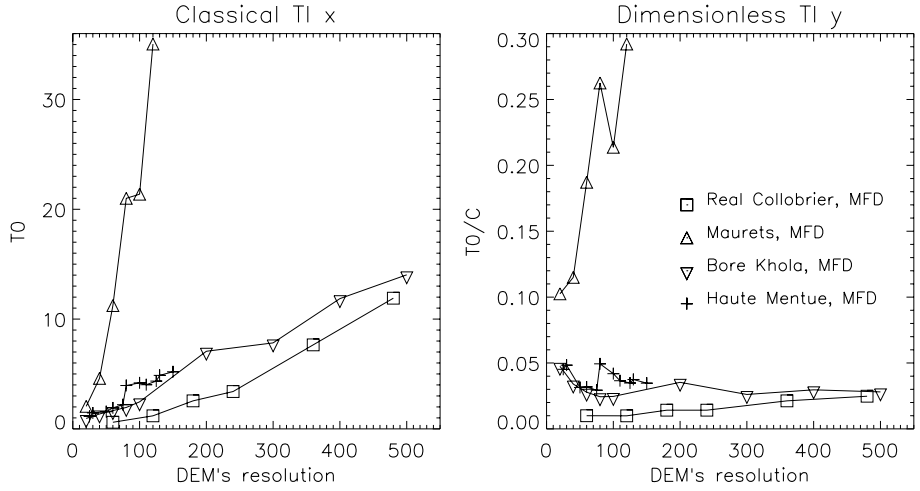

Fig. 3. Relationships between transmissivity T_0 or T_0/C and DEM resolution, in the classical and dimensionless TOPMODEL frameworks. Values come from Table 6, which also gives the corresponding correlation coefficients. Note that two of the six selected catchments (Sleepers-W3 and Kamishiiba) were excluded as their transmissivity values were outside the range covered in the other catchments (respectively much smaller and much larger).

Yet, T_0/C, the resulting rescaled transmissivity, is not completely invariant when DEM resolution varies, because of the calibration uncertainty on the one hand, and because other scale effects are involved on the other hand. The first one is that the mean TIs (whether classical or dimensionless) are also sensitive to terrain effects (related to discretization and smoothing), as analysed in Sect. 4.1. The second one is that the rescaling of transmissivity also compensates for changes in the TI distribution, as shown by Saulnier et al. (1997b) in the Maurets catchment (described in Table 3). These authors eventually proposed an efficient scaling factor for K_0, deduced from the differences in TI cumulative distributions when the DEM resolution changes.

The above scaling factors can be used to guide and facilitate the required recalibration of transmissivity when changing the DEM resolution, but it was later rather proposed to directly rescale the TI distribution, such as to limit the need to recalibrate the transmissivity.

4.3.2 Rescaling of the TI distribution

From a regression analysis using a sample of 50 quadrangles of $1°\times1°$ ($\simeq$7000 km^2) in the conterminous USA, Wolock and McCabe (2000) proposed a linear relationship to rescale the mean TIs obtained from a 1000-m resolution DEM ($\overline{x}_{1000}$) to values that would correspond to a 100-m resolution DEM ($\overline{x}_{100}$):

$$\overline{x}_{100} = -1.957 + 0.961\,\overline{x}_{1000}. \quad (39)$$

This linear regression is characterized by a high determination coefficient (R^2=0.93) and has been widely used (e.g. Kumar et al., 2000; Ducharne et al., 2000; Niu et al., 2005; Decharme and Douville, 2006). It can easily be extended to the dimensionless TI:

$$\overline{y}_{100} = 0.525 + 0.961\,\overline{y}_{1000}, \quad (40)$$

and the smaller y-intercept in Eq. (40) than in Eq. (39) confirms that $\overline{y}$ depends less on DEM resolution than $\overline{x}$, owing to the elimination of the numerical effect of DEM resolution. Figure 1 also suggests that a logarithmic relationship could perform better.

Mendicino and Sole (1997) analysed the simulations of 11 flood events by TOPMODEL in the Turbolo Creek (29 km^2, in Italy), using a 30-m resolution DEM, aggregated to coarser resolutions (90-m, 140-m and 270-m). They proposed a linear relationship between the mean TI and a spatial variability measure (SVM), which describes the topographic information content of the DEM following Shannon and Weaver (1949), and which depends on DEM resolution by a simple function of the number of grid cells.

This approach was further explored by Ibbitt and Woods (2004) in a 50-km^2 catchment in New Zealand, with similar results. These authors also provided evidence of a linear relationship between $\overline{x}(C)$ and $\log_{10}(C)$, which is perfectly consistent with the facts that $\overline{y} = \overline{x} - \ln C$ (from Eq. 18) and that $\overline{y}$ undergoes negligible variations with C, as shown in Sect. 4.2. The relationship between $\overline{x}(C)$ and $\log_{10}(C)$ is thus verified in the catchments of Table 5, the correlation coefficient exceeding 0.99 in all seven cases.

Combining the two linear relationships between $\overline{x}$, SVM and $\log_{10}(C)$, Ibbitt and Woods (2004) could define the DEM resolution that maximized the topographic information content: $\mathrm{SVM}(C) = 1 \Rightarrow C = 2$ cm, which corresponds to the scale of saturated conductivity measurements. Rescaling the

TI distribution to such resolution could render possible to use in situ measurements of the saturated hydraulic conductivity K_0, which is otherwise forbidden by the interplay between the DEM resolution, the mean classical TI and K_0.

Another method, aiming at rescaling the entire distribution of the classical TI instead of its mean, was proposed by Pradhan et al. (2006, 2008) in the Kamishiiba catchment (Table 3). The TI $x_{i,1}$ scaled at the target cell size C_1 from a coarser DEM with a cell size C_2 can be expressed as

$$x_{i,1} = \ln\left(\frac{a_{i,2} I_{f_R} C_1}{S_{i,1} I_{f_N} C_2}\right). \quad (41)$$

In this equation, I_{f_N} and I_{f_R} describe the terrain discretization effects on the upslope contributing area and contour length, respectively. They both depend on the two DEM cell sizes C_1 and C_2, and on the numbers of pixels at the coarser resolution in the upslope contributing area, $n_{i,2}$, and in the entire catchment, $n_{\text{out},2}$. Note that I_{f_R} was recently introduced in Pradhan et al. (2008) and is neglected in Pradhan et al. (2006). These authors also propose an interesting way to deduce the local slopes $S_{i,1}$ at the target resolution from the coarser DEM and a fractal method to introduce steepest slopes. Rearranging Eq. (41), by keeping in mind that I_{f_N} and I_{f_R} vary within the catchment, leads to

$$x_{i,1} = \ln\left(\frac{n_{i,2} I_{f_R}}{S_{i,1} I_{f_N}}\right) + \ln C_1. \quad (42)$$

This equation is very close to Eq. (18), as the first term in the right-hand side can be seen as a scaled dimensionless TI. It also reveals the three different DEM effects onto the classical TI distribution, previously separated in Table 2. The numerical effect, which has not been explicitly recognized by Pradhan et al. (2006, 2008), is quantified by $\ln C_1$. The discretization effect originates from I_{f_N} and I_{f_R}, and the smoothing effect from the rescaled slopes $S_{i,1}$. Note that these scaling techniques can be applied to the dimensionless as well as to the classical TI.

5 Conclusions

Replacing x_i, the classical TI of TOPMODEL, by the dimensionless TI $y_i = x_i - \ln C$, leads to reformulate TOPMODEL's main equations, then replaced by Eqs. (20) and (22). The principles and results of TOPMODEL are totally preserved in doing so but this reformulation offers several advantages. It firstly helps giving the units of all the variables (see Table 1), what is lacking in most papers about TOPMODEL, including the most cited ones (e.g. Beven and Kirkby, 1979; Sivapalan et al., 1987), probably by reluctance to use the logarithm of a length as a unit.

More importantly, the dependence of TOPMODEL equations on DEM cell size C becomes explicit, whereas it is hidden in the TI when using the classical formulation. This is a good way to raise awareness of hydrologists about the scale and resolution issues in the TOPMODEL framework. The mathematical dependence of TOPMODEL equations on C is then shifted from the classical TI, where it is related to the upslope contributing area per unit contour length, towards the equation of baseflow (Eq. 22), via T_0/C which can be defined as the transmissivity at saturation per unit contour length.

Accordingly, the mean dimensionless TI is free from the numerical effect, introduced in Sect. 4.1 as the direct effect of using the cell size in the definition of the classical TI. The influence of DEM resolution on the distribution of the dimensionless TI is thus restricted to the terrain effects, which result from terrain information loss at coarser resolutions, and which can be addressed for instance using the scaling methods proposed by Pradhan et al. (2006, 2008).

Nonetheless, based on six real-world case studies from the literature, we provide evidence that the DEM resolution influence on the mean classical TI $\overline{x}$ is largely dominated by the logarithmic numerical effect (Sect. 4.2). This results has important consequences, as:

- it sheds a new light upon the widely shared assumption according to which the dependence of the classical TI on DEM resolution mostly results from changes in terrain information (e.g. Sørensen and Seibert, 2007), which would probably be better identified by first removing the first-order numerical effect;

- the mean of the dimensionless TI is less sensitive to DEM resolution than the one of the classical TI, and it can be used as an efficient indicator to compare the topographic features of different catchments, almost regardless of DEM resolution;

- the transmissivity at saturation per unit contour length T_0/C is also more stable with DEM resolution than its counterpart T_0 in the classical framework. The need to recalibrate TOPMODEL when DEM resolution changes is thus markedly reduced using the dimensionless framework.

Finally, the dimensionless TI offers an interesting bridge between the two rescaling strategies developed within the classical TOPMODEL framework to reduce recalibration when DEM resolution changes, namely the rescaling of transmissivity and the rescaling of the TI distribution.

Acknowledgements. This paper benefited from fruitful discussions with Simon Gascoin and Pierre Ribstein, from the Laboratoire Sisyphe. The author also wishes to thank the editor, Francesc Gallart, and three reviewers, including Jan Seibert and Mike Kirkby, for their insightful comments, which helped a lot to improve the manuscript.

Edited by: F. Gallart

References

Ambroise, B., Beven, K. J., and Freer, J.: Toward a generalization of the TOPMODEL concepts: Topographic indices of hydrological similarity, Water Resour. Res., 32, 2135–2145, 1996.

Beven, K.: Hillslope runoff processes and flood frequency characteristics, in: Hillslope processes, edited by: Abrahams, S. D., Allen and Unwin, Boston, USA, 187–202, 1986.

Beven, K. and Freer, J.: A dynamic TOPMODEL, Hydrol. Process., 15, 1993–201, 2001a.

Beven, K. and Freer, J.: Equifinality, data assimilation, and uncertainty estimation in mechanistic modelling of complex environmental systems, J. Hydrol., 249, 11–29, 2001b.

Beven, K. and Kirkby, M. J.: A physically based variable contributing area model of basin hydrology, Hydrol. Sci. Bull., 24, 43–69, 1979.

Beven, K. J. and Binley, A. M.: The future of distributed models: model calibration and uncertainty prediction, Hydrol. Process, 6, 279–298, 1992.

Brasington, J. and Richards, K.: Interactions between model predictions, parameters and DTM scales for TOPMODEL, Comput. Geosci., 24, 299–314, doi:10.1016/S0098-3004(97)00081-2, 1998.

Brasington, J. and Richards, K.: Turbidity and suspended sediment dynamics in small catchments in the Nepal Middle Hills, Hydrol. Process., 14, 2559–2574, 2000.

Bruneau, P., Gascuel-Odoux, C., Robin, P., Mérot, P., and Beven, K.: Sensitivity to space and time resolution of a hydrological model using digital elevation data, Hydrol. Process., 9, 69–81, 1995.

Cappus: Etude des lois d'écoulement – Application au calcul et à la prevision des débits, Bassin expérimental d'Alrance, La Houille Blanche, 60, 493–520, 1960.

Chen, J. and Kumar, P.: Topographic Influence on the Seasonal and Interannual Variation of Water and Energy Balance of Basins in North America, J. Clim., 14, 1989–2014, 2001.

Curie, F., Gaillard, S., Ducharne, A., and Bendjoudi, H.: Geomorphological methods to characterize wetlands at the scale of the Seine watershed, Sci. Total. Environ., 375, 59–68, doi:10.1016/j.scitotenv.2006.12.013, 2007.

Decharme, B. and Douville, H.: Introduction of a sub-grid hydrology in the ISBA land surface model, Clim. Dyn., 26, 65–78, doi:10.1007/s00382-005-0059-7, 2006.

Duan, J. and Miller, N. L.: A generalized power function for the subsurface transmissivity profile in TOPMODEL, Water Resour. Res., 33, 2559–2562, 1997.

Ducharne, A., Koster, R. D., Suarez, M., Stieglitz, M., and Kumar, P.: A catchment-based approach to modeling land surface processes in a GCM – Part 2: Parameter estimation and model demonstration, J. Geophys. Res., 105, 24823–24838, 2000.

Famiglietti, J. S. and Wood, E. F.: Multiscale modeling of spatially variable water and energy balance processes, Water Resour. Res., 30, 3061–3078, 1994.

Franchini, M., Wendling, J., Obled, C., and Todini, E.: Physical interpretation and sensitivity analysis of the TOPMODEL, J. Hydrol., 175, 293–338, 1996.

Freer, J., Beven, K. J., and Ambroise, B.: Bayesian estimation of uncertainty in runoff prediction and the value of data: An application of the GLUE approach, Water Resour. Res., 32, 2161–2173, 1996.

Gallart, F., Latron, J., Llorens, P., and Beven, K.: Using internal catchment information to reduce the uncertainty of discharge and baseflow predictions, Adv. Water Resour., 30, 808–823, doi:10.1016/j.advwatres.2006.06.005, 2007.

Gascoin, S., Ducharne, A., Ribstein, P., Carli, M., and Habets, F.: Adaptation of a catchment-based land surface model to the hydrogeological setting of the Somme River basin (France), J. Hydrol., 368, 105–116, doi:10.1016/j.jhydrol.2009.01.039, 2009.

Higy, C. and Musy, A.: Digital terrain analysis of the Haute-Mentue catchment an scale effect for hydrological modelling with TOPMODEL, Hydrol. Earth Syst. Sci., 4, 225–237, 2000, http://www.hydrol-earth-syst-sci.net/4/225/2000/.

Holmgren, P.: Multiple flow direction algorithms for runoff modelling in grid based elevation models: An empirical evaluation, Hydrol. Process., 8, 327–334, 1994.

Ibbitt, R. and Woods, R.: Re-scaling the topographic index to improve the representation of physical processes in catchment models, J. Hydrol., 293, 205–218, doi:10.1016/j.jhydrol.2004.01.016, 2004.

Iorgulescu, I. and Jordan, J.-P.: Validation of TOPMODEL on a small Swiss catchment, J. Hydrol., 159, 255–273, 1994.

Jenson, S. K. and Domingue, J. O.: Extracting topographic structure from digital elevation data for geographic information system analysis, Photogramm. Eng. Rem. S., 54, 1593–1600, 1988.

Koster, R. D., Suarez, M., Ducharne, A., Stieglitz, M., and Kumar, P.: A catchment-based approach to modeling land surface processes in a GCM – Part 1: Model structure, J. Geophys. Res., 105, 24809–24822, 2000.

Kumar, P., Verdin, K. L., and Greenlee, S. K.: Basin level statistical properties of topographic index for North America, Adv. Water Resour., 23, 571–578, 2000.

Lee, G., Tachikawa, Y., and Takara, K.: Analysis of Hydrologic Model Parameter Characteristics Using Automatic Global Optimization Method, Annals of Disaster Prevention Research Institute, 67–80, 2006.

Mendicino, G. and Sole, A.: The information content theory for the estimation of the topographic index distribution used in TOPMODEL, Hydrol. Process., 11, 1099–1114, 1997.

Mérot, P., Ezzahar, B., Walter, C., and Aurousseau, P.: Mapping waterlogging of soils using digital terrain models, Hydrol. Process., 9, 27–34, 1995.

Nash, J. E. and Sutcliffe, J. V.: River flow forecasting through conceptual models. 1. A discussion of principles, J. Hydrol., 10, 282–290, 1970.

Niu, G.-Y., Yang, Z.-L., Dickinson, R. E., and Gulden, L. E.: A simple TOPMODEL-based runoff parameterization (SIMTOP) for use in global climate models, J. Geophys. Res., 110, D21 106, doi:10.1029/2005JD006111, 2005.

Obled, C., Wendling, J., and Beven, K.: The sensitivity of hydrological models to spatial rainfall patterns: an evaluation using observed data, J. Hydrol., 159, 305–333, 1994.

Pan, F., Peters-Lidard, C. D., Sale, M. J., and King, A. W.: Comparison of geographical information systems-based algorithms for computing the TOPMODEL topographic index, Water Resour. Res., 40, W06 303, doi:10.1029/2004WR003069, 2004.

Peters-Lidard, C. D., Zion, M. S., and Wood, E. F.: A soil-vegetation-atmosphere transfer scheme for modelling spatially variable water and energy balance processes, J. Geophys. Res., 102, 4303–4324, 1997.

Pradhan, N. R., Tachikawa, Y., and Takara, K.: A downscaling method of topographic index distribution for matching the scales of model application and parameter identification, Hydrol. Process., 20, 1385–1405, 2006.

Pradhan, N. R., Ogden, F. L., Tachikawa, Y., and Takara, K.: Scaling of slope, upslope area and soil water deficit: implications for transferability and regionalization in topographic index modeling, Water Resour. Res., 44, W12 421, doi:0.1029/2007WR006667, 2008.

Quinn, P., Beven, K., Chevallier, P., and Planchon, O.: The prediction of hillslope flow paths for distributed hydrological modelling using digital terrain models, Hydrol. Process., 5, 59–79, 1991.

Quinn, P., Beven, K., and Lamb, R.: The ln(a/tanB) index: how to calculate it and how to use it within the TOPMODEL framework, Hydrol. Process., 9, 161–182, 1995.

Saulnier, G.-M., Beven, K., and Obled, C.: Digital elevation analysis for distributed hydrological modelling: reducing scale dependence in effective hydraulic conductivity values, Water Resour. Res., 33, 2097–2101, 1997a.

Saulnier, G.-M., Obled, C., and Beven, K.: Analytical compensation between DTM grid resolution and effective values of saturated hydraulic conductivity within the TOPMODEL framework, Hydrological processes, 11, 1331–1346, 1997b.

Seibert, J. and McGlynn, B. L.: A new triangular multiple flow direction algorithm for computing upslope areas from gridded digital elevation models, Water Resour. Res., 43, W04 501, doi:0.1029/2006WR005128, 2006.

Shannon, C. E. and Weaver, W.: The Mathematical Theory of Communication, University of Illinois Press, Urbana, IL, 117 pp., 1949.

Sivapalan, M., Beven, K., and Wood, E. F.: On Hydrologic Similarity : 2. A Scaled Model of Storm Runoff Production, Water Resour. Res., 23, 2266–2278, 1987.

Sørensen, R. and Seibert, J.: Effects of DEM resolution on the calculation of topographical indices: TWI and its components, J. Hydrol., 347, 79–89, 2007.

Sørensen, R., Zinko, U., and Seibert, J.: On the calculation of the topographic wetness index: evaluation of different methods based on field observations, Hydrol. Earth Syst. Sci., 10, 101–112, 2006, http://www.hydrol-earth-syst-sci.net/10/101/2006/.

Stieglitz, M., Rind, M., Famiglietti, J., and Rosenzweig, C.: An efficient approach to modeling the topographic control of surface hydrology for regional and global modeling, J. Clim., 10, 118–137, 1997.

Tallaksen, L. M.: A review of baseflow recession analysis, J. Hydrol., 165, 349–370, doi:10.1016/0022-1694(94)02540-R, 1995.

Tarboton, D. G.: A new method for the determination of flow directions and upslope areas in grid digital elevation models, Water Resour. Res., 33, 309–319, 1997.

Valeo, C. and Moin, S. M. A.: Grid-resolution effects on a model for integrating urban and rural areas, Hydrol. Process., 14, 2505–2525, 2000.

Wolock, D. and McCabe, G.: Differences in topographic characteristics computed from 100- and 1000-meter resolution digital elevation model data, Hydrol. Process., 14, 987–1002, 2000.

Wolock, D. M. and McCabe, G. J.: Comparison of single and multiple flow direction algorithms for computing topographic parameters in TOPMODEL, Water Resour. Res., 31, 1315–1324, 1995.

Wolock, D. M. and Price, C. V.: Effects of digital elevation model map scale and data resolution on a topography-based watershed model, Water Resour. Res., 30, 3041–3052, 1994.

Wu, S., Li, J. and Huang, G. H.: Modeling the effects of elevation data resolution on the performance of topography-based watershed runoff simulation, Environ. Modell. Softw., 22, 1250–1260, doi:10.1016/j.envsoft.2006.08.001, 2007.

Zhang, W. and Montgomery, D. R.: Digital elevation model grid size, landscape representation, and hydrologic simulations, Water Resour. Res., 30, 1019–1028, 1994.